Nano Research 2014, 7(8): 1195–1204
DOI 10.1007/s12274-014-0482-3
Research Article
ISSN 1998-0124
CN 11-5974/O4

Surface properties of encapsulating hydrophobic nanoparticles regulate the main phase transition temperature of lipid bilayers: A simulation study

Xubo Lin and Ning Gu (✉)

State Key Laboratory of Bioelectronics and Jiangsu Key Laboratory for Biomaterials and Devices, School of Biological Science & Medical Engineering, Southeast University, Nanjing 210096, China

Received: 24 February 2014
Revised: 14 April 2014
Accepted: 17 April 2014

KEYWORDS
lipid bilayer,
phase transition,
nanoparticle,
surface roughness,
density,
surface molecules

ABSTRACT

The main phase transition temperature of a lipid membrane, which is vital for its biomedical applications such as controllable drug release, can be regulated by encapsulating hydrophobic nanoparticles into the membrane. However, the exact relationship between surface properties of the encapsulating nanoparticles and the main phase transition temperature of a lipid membrane is far from clear. In the present work, we performed coarse-grained molecular dynamics simulations to meet this end. The results show the surface roughness of nanoparticles and the density of surface-modifying molecules on the nanoparticles are responsible for the regulation. Increasing the surface roughness of the nanoparticles increases the main phase transition temperature of the lipid membrane, whereas it can be decreased in a nonlinear way via increasing the density of surface-modifying molecules on the nanoparticles. The results may provide insights for understanding recent experimental studies and promote the applications of nanoparticles in controllable drug release by regulating the main phase transition temperature of lipid vesicles.

1 Introduction

Hybrid lipid vesicle–hydrophobic nanoparticle (NP) systems have attracted broad interest based on their advantages in diagnostic and therapeutic applications [1]. NPs can stabilize the lipid vesicle [2], modulate the phase behavior of the lipid vesicle [3, 4], and trigger the lipid vesicle to release its inclusions under an external field for controlled drug release [5–7]. Furthermore, lipids may improve the biocompatibility of NPs, which promotes the biomedical applications of hydrophobic NPs such as in medical imaging [8, 9].

The synthesis of hybrid lipid vesicle–hydrophobic NP systems has been extensively studied. Theoretically, neutral hydrophobic NPs of size less than or comparable to the membrane thickness can be easily encapsulated into the bilayer of the lipid vesicle [10–12]. Besides, shape also affects the efficiency of

Address correspondence to guning@seu.edu.cn

encapsulation [13, 14]. Experimentally, for one thing, the encapsulation of certain NPs can be achieved by modifying proper molecules to the surface of NPs [15]. For another, synthesizing inorganic NPs of specific size, shape, surface chemistry has already become possible [16–19], which ensures the success of the encapsulation. For example, Rasch et al. [20, 21] coated Au NPs (diameter less than 2 nm) with dodecanethiol, mixed the products with lipids, and successfully obtained hybrid systems using the self-assembly method. Lee et al. [22] functionalized NPs with hydrophobic and hydrophilic ligands and realized the incorporation of NPs with size greatly exceeding the bilayer thickness.

Since NPs with various properties can be incorporated into the lipid bilayer, many further studies have focused on the effects of NPs on the lipid bilayer. Park et al. [23] entrapped Ag NPs into the hydrophobic region of dipalmitoylphosphatidyl-choline (DPPC) liposomes and found Ag NPs can increase membrane fluidities above the main phase transition temperature of DPPC molecules (41 ℃). They further found Au NPs have the similar effects [24]. Bothun et al. [25] embedded Ag-decanethiol NPs into the bilayer and demonstrated, using differential scanning calorimetry and fluorescence anisotropy, that increasing the nanoparticle concentration suppresses the lipid pretransition temperature, reduces the main phase transition temperature, and disrupts gel phase bilayers. Recently, they further found that a high loading of embedded stearylamine (SA)-stabilized Au NPs induced large increases in the main phase transition temperature of DPPC/dipalmitoylphosphatidylglycerol (DPPG) vesicles [26]. They ascribed this behavior to the cooperative effects of excess free SA ligands and NPs. As a result, the main phase transition temperature of the lipid bilayer can be either reduced or increased by encapsulating NPs with specific surface properties. However, the precise relationship between surface properties of NPs and changes in the main phase transition temperature is far from being fully understood, and this is the focus of this work.

The main phase transition process (gel-to-fluid phase transition) is primarily a cooperative rotameric disordering of the hydrocarbon chains, which is determined by combined excluded volume interactions and attractive van der Waals interchain interactions [27]. Both these two main interactions can both be properly reproduced using the MARTINI force field [28]. Hence, it is valid to use the MARTINI force field to study the main phase transition of lipid membranes. Several recent simulation studies have validated the applicability of the MARTINI force field to study phase transition process of lipid membranes [29–33]. It is worth mentioning that the size of the lipid vesicle for the hybrid NP–vesicle system generally exceeds hundreds of nanometers in diameter and the small local region of the hybrid system can be approximated as a planar lipid bilayer (about tens of nanometers in size) encapsulating the hydrophobic NPs. Therefore, in this study, we focus on the effects of surface chemistry—such as surface roughness and surface ligand density on the hydrophobic NPs—on changes in the main phase transition temperature of planar lipid bilayer.

2 Model and simulation details

Briefly, the MARTINI CG model is based on a four-to-one mapping, i.e., on average four heavy atoms are represented by a single interaction site. Only four main types of interaction sites are defined: Polar (P), nonpolar (N), apolar (C), and charged (Q). Each particle type has a number of subtypes, which allow for a more accurate representation of the chemical nature of the underlying atomic structure. Within a main type, subtypes are either distinguished by a letter denoting the hydrogen-bonding capabilities ("d" donor, "a" acceptor, "da" both, and "0" none), or by a number indicating the degree of polarity (from 1, low polarity, to 5, high polarity). A shifted Lennard–Jones (LJ) 12–6 potential energy function

$$U_{\mathrm{LJ}}(r) = 4\varepsilon_{ij}\left[\left(\frac{\sigma_{ij}}{r}\right)^{12} - \left(\frac{\sigma_{ij}}{r}\right)^{6}\right] \quad (1)$$

(σ_{ij} representing the closest distance of approach between two particles and ε_{ij} the strength of their interactions) and a shifted Coulombic potential energy function

$$U_{\mathrm{el}}(r) = \frac{q_i q_j}{4\pi\varepsilon_0\varepsilon_{\mathrm{r}} r} \quad (2)$$

(relative dielectric constant ε_r=15 for explicit screening) are used to describe the non-bonded interactions. A weak harmonic potential

$$V_{\text{bond}}(R) = \frac{1}{2}K_{\text{bond}}(R - R_{\text{bond}})^2 \quad (3)$$

(an equilibrium distance $R_{\text{bond}} = \sigma = 0.47$ nm and a force constant of $K_{\text{bond}} = 1,250\ \text{kJ}\cdot\text{mol}^{-1}\cdot\text{nm}^{-2}$) is applied for the bonded interactions. A weak harmonic potential

$$V_{\text{angle}}(\theta) = \frac{1}{2}K_{\text{angle}}\{\cos(\theta) - \cos(\theta_0)\}^2 \quad (4)$$

is used for the angles to represent chain stiffness. For aliphatic chains, the force constant $K_{\text{angle}} = 25\ \text{kJ}\cdot\text{mol}^{-1}$ and the equilibrium bond angle $\theta_0 = 180°$; for the cis double bond, $K_{\text{angle}} = 35\ \text{kJ}\cdot\text{mol}^{-1}$ and $\theta_0 = 120°$. More details can be found in the Electronic Supplementary Material (ESM) or in the paper by Marrink et al. [28].

Considering that the size of the lipid vesicle for the hybrid NP–vesicle system generally exceeds hundreds of nanometers in diameter, the small local region of the hybrid system can be approximated as a planar lipid bilayer encapsulating hydrophobic NPs. In this study, our systems each include a planar DPPC bilayer of 512 DPPC molecules, 17,920 CG water molecules, and a NP. The CG representations of DPPC and water molecules are the same as in the literature [28]. In this work, we focus on physical surface properties, such as surface roughness and surface molecule density, rather than the surface chemistry of NPs. Hence, we choose a C1-type bead, which is the same as the tails of DPPC molecules (Fig. 1(a)), to build hydrophobic NPs and ligand molecules. Beads are placed evenly on the concentric spherical surfaces to obtain a NP with a smooth surface (Fig. 1(b)); beads are stacked in a face-centered cubic (FCC) manner to form a NP with a rough surface (Fig. 1(c)), and all beads of NP within 1 nm are constrained by a bond to ensure a rigid NP. This modeling method for a nonspecific NP has been widely used with the MARTINI and other coarse-grained models [11, 34–44] and helps to elucidate the general effects of the properties of NPs (such as size, shape, surface chemistry, and stiffness) on its interactions with the lipid bilayer. As for the ligand molecule, we choose a three-bead model, the length

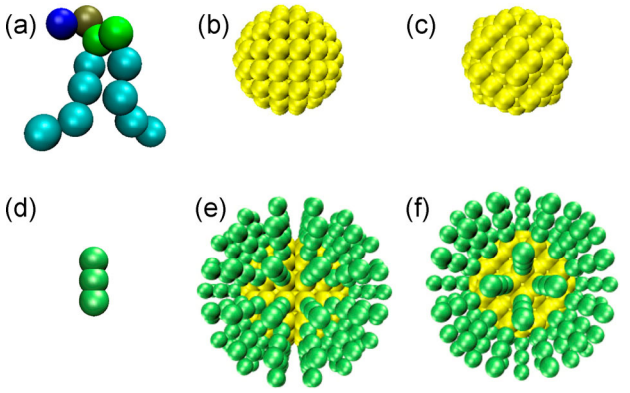

Figure 1 Snapshots of (a) a coarse-grained DPPC molecule, (b) a smooth NP, (c) a rough NP, (d) a ligand molecule, (e) a smooth NP with ligand molecules, and (f) a rough NP with ligand molecules. The CG beads of NP (yellow) and ligand molecule (lime) have the same hydrophobic properties as that of the DPPC tail (cyan).

of which is close to that of 12-carbon straight-chain alkanes. 0%, 33%, 50%, 100% of the surface beads of NPs (diameter d = 3 nm) are evenly modified with ligand molecules to realize different ligand densities on the surface. In addition, NPs (d = 4 nm) are considered as a control group to evaluate the effects of size increase induced by surface ligands.

A hydrophobic NP was first placed in the water near the DPPC bilayer (the minimum distance between NP and the bilayer is 0.5 nm) and the system was relaxed for 200 ns at a temperature of T = 335 K. Then, an external force was exerted on NP to drag it into the hydrophobic region of the DPPC bilayer. (The dynamics of NPs penetrating into a lipid bilayer has been widely probed. Hence, we use an external force just to obtain conformation of the lipid bilayer with the encapsulated NP.) All NPs can be easily embedded in the DPPC bilayer to form stable hybrid systems. The hybrid system was cooled by ΔT = 5 K step by step until 280 K. The output configuration at T was used as starting input for the system at T–ΔT and a 400 ns equilibrium run was performed at each temperature with last 100 ns for data analysis (at each temperature, the system can reach equilibrium within 300 ns). The final conformation at T =280 K was used as the initial state for the gel-to-fluid phase transition simulation (heating process), which had a similar procedure as mentioned above but in the reverse direction.

For all simulations, a cutoff of 1.2 nm was used for van der Waals (vdW) interactions, and the Lennard–Jones potential was smoothly shifted to zero between 0.9 nm and 1.2 nm to reduce cutoff noise. For electrostatic interactions, the Coulombic potential, with a cutoff of 1.2 nm, was smoothly shifted to zero from 0 to 1.2 nm. The relative dielectric constant was 15, which is the default value of the force field [28]. DPPC, water and NPs were coupled separately to Berendsen heat baths [45] at T, with a coupling constant τ = 1 ps. The monolayer compression was simulated using semiisotropic pressure coupling (Berendsen coupling scheme [45], with a coupling constant of 4 ps, compressibility in the lateral direction of 5×10^{-5} bar^{-1} and in the normal direction of zero). Each of the simulations was performed for 400 ns with a time step of 40 fs. The neighbor list for non-bonded interactions was updated every 10 steps. Snapshots of the simulation system in this paper were all rendered by the Visual Molecular Dynamics (VMD) software [46]. All simulations were performed with the GROMACS simulation package [47].

3 Results and discussion

3.1 Phase transition kinetics of the pure DPPC bilayer

The different phases of the pure DPPC bilayer have been studied by various experimental methods. It is known that the DPPC bilayer can exist in many phases such as the fluid phase, the ripple phase, the gel phase, the subgel phase, the nonlamellar cubic phase, and the inverse hexagonal phase [30, 48, 49]. The transition from the ripple phase to the fluid phase is defined as the main phase transition. The occurrence of the main phase transition is always accompanied by sudden shifts in parameters such as the volume, the area per lipid, and the lipid tail order parameter, which can be easily quantified both in experiments [48, 49] and simulations [29–32, 50].

In order to capture the process of the main phase transition, the area per lipid (Fig. 4) and the lipid order parameter (Fig. 5) were calculated. Above T = 315 K, the area per lipid experiences a sudden increase and the lipid order parameter showed a sudden decrease, which characterizes the occurrence of the main phase transition. Hence, we can obtain the main phase transition temperature (T_m) of the pure DPPC bilayer as about T_m = 315 K from our simulation results, which is similar to gel-to-fluid simulations reported by Rodgers et al. [30]. It is worth mentioning that this value is quite different from the value of 295 ± 5 K calculated by the developer of the MARTINI force field [51]. By carefully comparing the differences between our simulation systems and related systems, we can ascribe the difference between the results mainly to the system size together with the force field itself. 295 ± 5 K is the result for larger systems using the initial version of the MARTINI force field [51, 52] while 315 K is the value obtained for smaller systems using the improved MARTINI force field [28–30]. To enable direct comparison, we enlarged the smaller systems to four-fold systems (2,048 DPPC molecules), and found the main phase transition temperature of the pure DPPC bilayer was reduced to 310 K (Fig. S4 in the ESM). But the trends in the effects of NPs are the same both for the smaller and the larger systems, which validates our results of smaller systems.

We further calculated the two-dimensional (2D) phase map of the DPPC bilayer to capture the details. The 2D phase map was constructed using the lipid order parameters of DPPC molecules as described in our previous work [36]. As shown in Fig. 2(a), the 2D phase map clearly shows the lipid tail order parameter of the DPPC bilayer at different temperatures. At T = 280 K, the tail order parameters of all lipids are large, representing consistent orientation of lipid tails, which corresponds to the gel phase. On increasing the temperature to 290 K, a liquid-disordered lipid nanodomain appears (the green region in the images at 290–315 K in Fig. 2(a)). The snapshot (Fig. 2(b)) further shows this is a ripple-like phase, which is similar to "the intermediate phase" reported by Rodgers et al. [30]. Then above 315 K, the whole map is green, corresponding to a lipid-disordered state and thus the fluid phase. Our simulation and analysis methods reproduced the main phase transition of the pure DPPC bilayer very well.

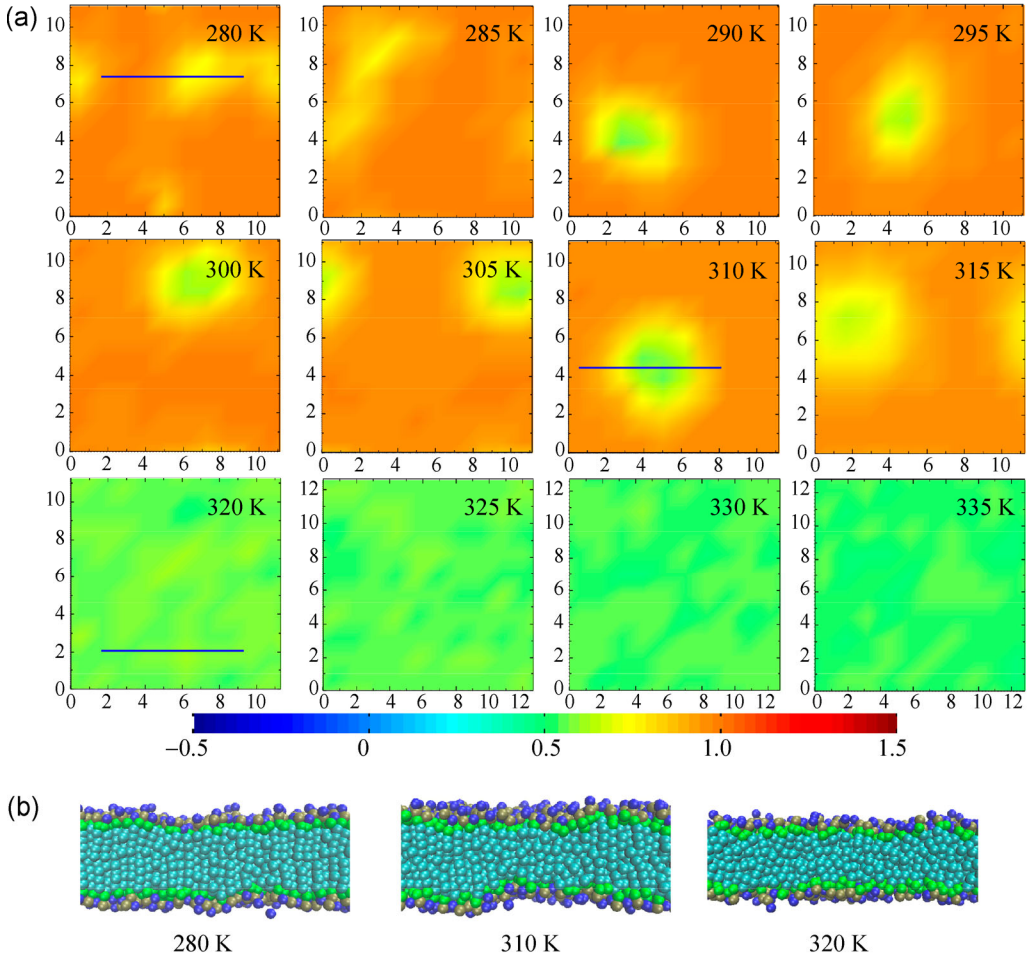

Figure 2 (a) Two-dimensional (2D) phase map of a pure DPPC bilayer during the gel-to-fluid phase transition, where different colors correspond to different order parameters as shown in the color bar; (b) Snapshots of section views of DPPC bilayer marked using the blue line in (a). The DPPC bilayer experiences transitions from a gel phase (280 K), to ripple-like phase (290 K), to fluid phase (320 K).

3.2 Phase transition temperature of the DPPC bilayer encapsulating hydrophobic NPs

As has been reported, hydrophobic NPs with size less than or comparable to the membrane thickness can be easily encapsulated in a lipid bilayer [10–12]. In the present work, our focus is the relationship between the main phase transition temperature of the DPPC bilayer and the surface properties of encapsulating NPs rather than the penetration dynamics of different NPs. The latter has been widely studied by many other researchers [11, 34–44]. Hence, we just perform pulling simulations to drag NPs into the hydrophobic region of the DPPC bilayer at T = 335 K. All the NPs can be easily encapsulated into the DPPC bilayer and remain stable in the hydrophobic region of the bilayer throughout the simulation time. Then the obtained NP–bilayer complex systems were cooled to T = 280 K as the initial systems for the main phase transition simulations.

With the encapsulation of hydrophobic NPs, the orientation of DPPC molecules adjacent to NPs are disrupted (Fig. 3 and Fig. S1 in the ESM), which is consistent with the reconstruction of neighboring DPPC molecules induced by NPs reported in the experiments of Wang et al. [3]. This disruption is similar at all temperatures considered in our simulations. Furthermore, no liquid–disordered lipid nanodomain far from NPs exists before the main phase transition. This does not represent the disappearance of the ripple-like phase, since NPs may prefer to interact with the fluid phase lipid bilayer rather than the gel phase

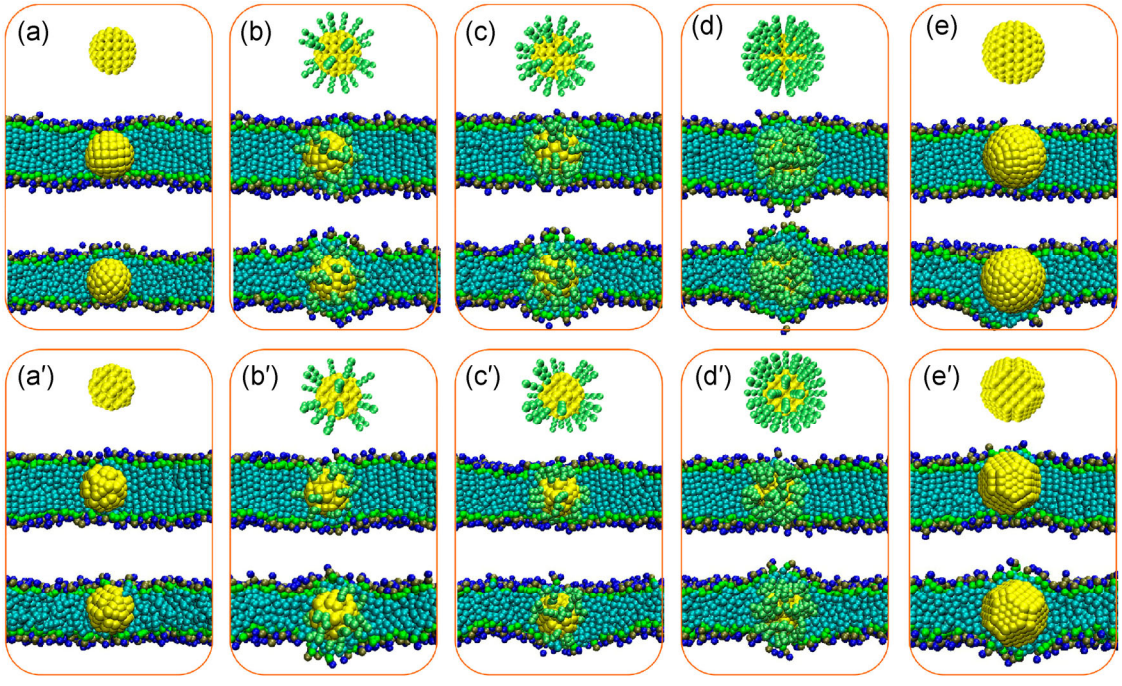

Figure 3 Snapshots of a smooth NP of (a) 3 nm size (0% ligands), (b) 3 nm (33% ligands), (c) 3 nm (50% ligands), (d) 3 nm (100% ligands), (e) 4 nm (0% ligands) and their encapsulation in the DPPC bilayer of the gel phase (middle of the orange box) and the fluid phase (bottom of the orange box). (a')–(e') are the corresponding cases for rough NPs. The colors of DPPC and NPs are the same as in Fig. 1. Water molecules are not shown for clarity.

lipid bilayer [53]. In other words, the liquid–disordered lipid nanodomain may appear at the location of the NPs. In addition, it is worth mentioning that the disruption does not dominate the whole phase behavior at each specific temperature, and all the hydrophobic NPs can remain stable in the DPPC bilayers of both the gel phase and the fluid phase during the whole gel-to-fluid phase transition simulations (Figs. S2 and S3 in the ESM).

The area per lipid and the lipid tail order parameter were calculated to study the phase transition kinetics of the DPPC bilayer encapsulating NPs (Figs. 4 and 5). Lipids of the fluid phase are characterized by larger area per lipid and smaller lipid tail order parameter compared with the corresponding values for the gel phase. The sudden increase of the area per lipid and the sudden decrease of lipid tail order parameter correspond to the occurrence of the gel-to-fluid phase transition. In general, Figs. 4 and 5 show that the main phase transition temperature can be either increased or decreased by encapsulating NPs with appropriate surface roughness and density of surface ligand molecules into the DPPC bilayer. Figure 6 further summarizes the effects of surface roughness and the density of ligand molecules on the main phase transition temperature of the DPPC bilayer. For smooth NPs, addition of 3 nm (0% ligand) NPs has no effects on the T_m. With the increase of the density of ligand molecules (from 0 to 100%), T_m first decreases to a low value and then increases slightly. Addition of 4 nm (0% ligand) NPs also has little effect on the T_m, which therefore excludes any effects of the size increase induced by ligand molecules. For rough NPs, 3 nm (0% ligand) NPs increase T_m. The effect of the density of ligand molecules is similar to that for smooth NPs. With the increase in number of surface ligand molecules, the effects of adding NPs gradually become dominated by the ligand molecules (as in the cases of 50% and 100% ligands). These results are supported by some recent experimental studies on the effects of hydrophobic NPs on the main phase transition temperature of lipid bilayers [25, 26]. For example, Bothun [25] embedded Ag-decanethiol NPs into a DPPC bilayer and found the main phase transition

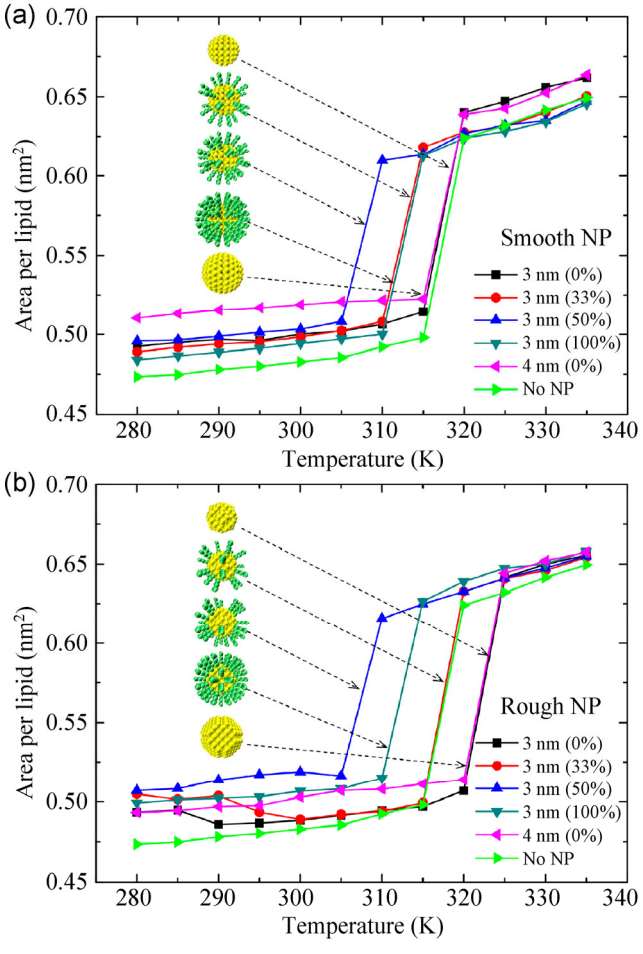

Figure 4 Variation of the area per lipid during the main phase transition process for the DPPC bilayer encapsulating (a) smooth NPs and (b) rough NPs. The green line is for the case of the pure DPPC bilayer.

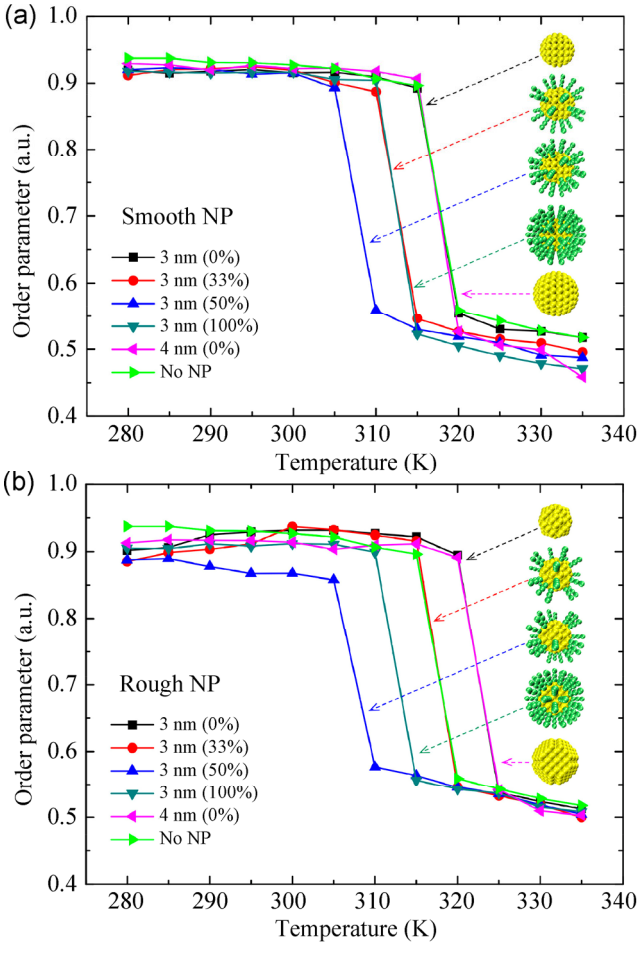

Figure 5 Variation of order parameter during the main phase transition process for DPPC bilayer encapsulating (a) smooth NPs and (b) rough NPs. The green line is for the case of the pure DPPC bilayer.

temperature was reduced. Decanethiol molecules modify the surface of Ag NPs via covalent interactions to form Ag–decanethiol NPs, whilst covalent interactions are strong enough to keep decanethiol molecules on the surface of Ag NPs while in the hydrophobic region of the DPPC bilayer. Here, Ag NPs with sufficient surface molecules can bring down the main phase transition temperature of the DPPC bilayer, which is consistent with our simulations. More recently, White et al. [26] demonstrated that the main phase transition temperature of DPPC/DPPG vesicles can be markedly increased by encapsulating stearylamine (SA)-stabilized Au NPs. SA molecules are attached to the surface of Au NPs due to electrostatic interactions. However, it is well documented that surface roughness has influence on the attachment and detachment of

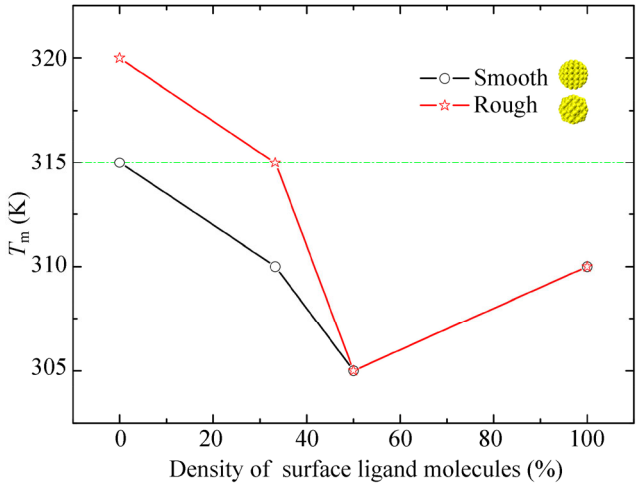

Figure 6 The relationship between the main phase transition temperature (T_m) of the DPPC bilayer and the surface properties of its encapsulating NPs. The green line (315 K) is for the case of the pure DPPC bilayer.

colloids on surfaces [54–56]. Hence, SA molecules may detach from the surface of NPs to form naked Au NPs in the hydrophobic region of the DPPC/DPPG bilayer. The naked Au NPs, which have rougher surface, further increase the main phase transition temperature of the lipid bilayer together with the free SA molecules. The results of the FCC-stacked rough NPs in our simulations are completely consistent with the behavior of Au NPs mentioned above.

4 Conclusions

We have performed coarse-grained molecular dynamics simulations to probe the effects of encapsulated NPs on the main phase transition temperature of a DPPC bilayer. The results show that tuning the properties of NPs—such as surface roughness and the density of ligand molecules—can help modulate the main phase transition temperature of the DPPC bilayer. Increasing the surface roughness of NPs raises the main phase transition temperature of the DPPC bilayer, while increasing the density of surface ligand molecules of NPs causes the main phase transition temperature of DPPC bilayer to initially decrease and then increase. The results may provide insights into optimizing the design of hybrid NP–vesicle systems and thus promote their biomedical applications in drug release systems and other areas.

Acknowledgements

We acknowledge the support of this research from the National Important Basic Research Program of China (No. 2011CB933503), the National Natural Science Foundation of China (No. 61127002), the Basic Research Program of Jiangsu Province (No. BK2011036), and the Outstanding Ph.D. Student Program of China's Ministry of Education.

Electronic Supplementary Material: Supplementary material (details about the MARTINI force field, two-dimensional phase maps of the DPPC bilayer encapsulating NPs at different temperatures, system size effects) is available in the online version of this article at http://dx.doi.org/10.1007/s12274-014-0482-3.

References

[1] Al-Jamal, W.; Kostarelos, K. Liposome-nanoparticle hybrids for multimodal diagnostic and therapeutic applications. *Nanomedicine* **2007**, *2*, 85–98.

[2] Zhang, L. F.; Granick, S. How to stabilize phospholipid liposomes (using nanoparticles). *Nano Lett.* **2006**, *6*, 694–698.

[3] Wang, B.; Zhang, L. F.; Bae, S. C.; Granick, S. Nanoparticle-induced surface reconstruction of phospholipid membranes. *Proc. Natl. Acad. Sci. U.S.A.* **2008**, *105*, 18171–18175.

[4] Urban, A. S.; Fedoruk, M.; Horton, M. R.; Rädler, J. O.; Stefani, F. D.; Feldmann, J. Controlled nanometric phase transitions of phospholipid membranes by plasmonic heating of single gold nanoparticles. *Nano Lett.* **2009**, *9*, 2903–2908.

[5] Chen, Y. J.; Bose, A.; Bothun, G. D. Controlled release from bilayer-decorated magnetoliposomes via electromagnetic heating. *ACS Nano* **2010**, *4*, 3215–3221.

[6] Amstad, E.; Kohlbrecher, J.; Müller, E.; Schweizer, T.; Textor, M.; Reimhult, E. Triggered release from liposomes through magnetic actuation of iron oxide nanoparticle containing membranes. *Nano Lett.* **2011**, *11*, 1664–1670.

[7] An, X. Q.; Zhan, F.; Zhu, Y. Y. Smart photothermal-triggered bilayer phase transition in AuNPs–liposomes to release drug. *Langmuir* **2013**, *29*, 1061–1068.

[8] Gopalakrishnan, G.; Danelon, C.; Izewska, P.; Prummer, M.; Bolinger, P.-Y.; Geissbhler, I.; Demurtas, D.; Dubochet, J.; Vogel, H. Multifunctional lipid/quantum dot hybrid nanocontainers for controlled targeting of live cells. *Angew. Chem. Int. Ed.* **2006**, *45*, 5478–5483.

[9] Marshall, J. D.; Schnitzer, M. J. Optical strategies for sensing neuronal voltage using quantum dots and other semiconductor nanocrystals. *ACS Nano* **2013**, *7*, 4601–4609.

[10] Qiao, R.; Roberts, A. P.; Mount, A. S.; Klaine, S. J.; Ke, P. C. Translocation of C_{60} and its derivatives across a lipid bilayer. *Nano Lett.* **2007**, *7*, 614–619.

[11] Lin, X. B.; Li, Y.; Gu, N. Nanoparticle's size effect on its translocation across a lipid bilayer: A molecular dynamics simulation. *J. Comput. Theor. Nanosci.* **2010**, *7*, 269–276.

[12] Ginzburg, V. V.; Balijepalli, S. Modeling the thermodynamics of the interaction of nanoparticles with cell membranes. *Nano Lett.* **2007**, *7*, 3716–3722.

[13] Nangia, S.; Sureshkumar, R. Effects of nanoparticle charge and shape anisotropy on translocation through cell membranes. *Langmuir* **2012**, *28*, 17666–17671.

[14] Wang, H. M.; Michielssens, S.; Moors, S. L. C.; Ceulemans, A. Molecular dynamics study of dipalmitoylphosphatidyl-choline lipid layer self-assembly onto a single-walled carbon nanotube. *Nano Res.* **2009**, *2*, 945–954.

[15] Lehn, R. C. V.; Atukorale, P. U.; Carney, R. P.; Yang, Y. S.; Stellacci, F.; Irvine, D. J.; Alexander-Katz, A. Effect of particle diameter and surface composition on the spontaneous fusion of monolayer-protected gold nanoparticles with lipid bilayers. *Nano Lett.* **2013**, *13*, 4060–4067.

[16] Grzelczak, M.; Perez-Juste, J.; Mulvaney, P.; Liz-Marzan, L. M. Shape control in gold nanoparticle synthesis. *Chem. Soc. Rev.* **2008**, *37*, 1783–1791.

[17] Alkilany, A. M.; Lohse, S. E.; Murphy, C. J. The gold standard: Gold nanoparticle libraries to understand the nano–bio interface. *Acc. Chem. Res.* **2013**, *46*, 650–661.

[18] Sun, Y. Controlled synthesis of colloidal silver nanoparticles inorganic solutions: Empirical rules for nucleation engineering. *Chem. Soc. Rev.* **2013**, *42*, 2497–2511.

[19] Kim, S. T.; Saha, K.; Kim, C.; Rotello, V. M. The role of surface functionality in determining nanoparticle cytotoxicity. *Acc. Chem. Res.* **2013**, *46*, 681–691.

[20] Rasch, M. R.; Rossinyol, E.; Hueso, J. L.; Goodfellow, B. W.; Arbiol, J.; Korgel, B. A. Hydrophobic gold nanoparticle self-assembly with phosphatidylcholine lipid: Membrane-loaded and Janus vesicles. *Nano Lett.* **2010**, *10*, 3733–3739.

[21] Rasch, M. R.; Yu, Y.; Bosoy, C.; Goodfellow, B. W.; Korgel, B. A. Chloroform-enhanced incorporation of hydrophobic gold nanocrystals into dioleoylphosphatidylcholine (DOPC) vesicle membranes. *Langmuir* **2012**, *28*, 12971–12981.

[22] Lee, H.-Y.; Shin, S. H. R.; Abezgauz, L. L.; Lewis, S. A.; Chirsan, A. M.; Danino, D. D.; Bishop, K. J. M. Integration of gold nanoparticles into bilayer structures via adaptive surface chemistry. *J. Am. Chem. Soc.* **2013**, *135*, 5950–5953.

[23] Park, S.-H.; Oh, S.-G.; Mun, J.-Y.; Han, S.-S. Effects of silver nanoparticles on the fluidity of bilayer in phospholipid liposome. *Colloid Surf. B* **2005**, *44*, 117–122.

[24] Park, S.-H.; Oh, S.-G.; Mun, J.-Y.; Han, S.-S. Loading of gold nanoparticles inside the DPPC bilayers of liposome and their effects on membrane fluidities. *Colloid Surf. B* **2006**, *48*, 112–118.

[25] Bothun, G. D. Hydrophobic silver nanoparticles trapped in lipid bilayers: Size distribution, bilayer phase behavior, and optical properties. *J. Nanobiotechnol.* **2008**, *6*, 13.

[26] White, G. V.; Chen, Y. J.; Roder-Hanna, J.; Bothun, G. D.; Kitchens, C. L. Structural and thermal analysis of lipid vesicles encapsulating hydrophobic gold nanoparticles. *ACS Nano* **2012**, *6*, 4678–4685.

[27] Nagle, J. F. Theory of the main lipid bilayer phase transition. *Ann. Rev. Phys. Chem.* **1980**, *31*, 157–195.

[28] Marrink, S. J.; Risselada, H. J.; Yefimov, S.; Tieleman, D. P.; de Vries, A. H. The MARTINI force field: Coarse grained model for biomolecular simulations. *J. Phys. Chem. B* **2007**, *111*, 7812–7824.

[29] Ramalho, J. P. P.; Gkeka, P.; Sarkisov, L. Structure and phase transformations of DPPC lipid bilayers in the presence of nanoparticles: Insights from coarse-grained molecular dynamics simulations. *Langmuir* **2011**, *27*, 3723–3730.

[30] Rodgers, J. M.; Sørensen, J.; de Meyer, F. J.-M.; Schiøtt, B.; Smit, B. Understanding the phase behavior of coarse-grained model lipid bilayers through computational calorimetry. *J. Phys. Chem. B* **2012**, *116*, 1551–1569.

[31] Hakobyan, D.; Heuer, A. Phase separation in a lipid/cholesterol system: Comparison of coarse-grained and united-atom simulations. *J. Phys. Chem. B* **2013**, *117*, 3841–3851.

[32] Waheed, Q.; Tjörnhammar, R.; Edholm, O. Phase transitions in coarse-grained lipid bilayers containing cholesterol by molecular dynamics simulations. *Biophys. J.* **2012**, *103*, 2125–2133.

[33] Marrink, S. J.; Tieleman, D. P. Perspective on the Martini model. *Chem. Soc. Rev.* **2013**, *42*, 6801–6822.

[34] Li, Y.; Chen, X.; Gu, N. Computational investigation of interaction between nanoparticles and membranes: Hydrophobic/hydrophilic effect. *J. Phys. Chem. B* **2008**, *112*, 16647–16653.

[35] Li, Y.; Gu, N. Thermodynamics of charged nanoparticle adsorption on charge-neutral membranes: A simulation study. *J. Phys. Chem. B* **2010**, *114*, 2749–2754.

[36] Lin, X. B.; Wang, C. L.; Wang, M.; Fang, K.; Gu, N. Computer simulation of the effects of nanoparticles' adsorption on the properties of supported lipid bilayer. *J. Phys. Chem. C* **2012**, *116*, 17960–17968.

[37] Vácha, R.; Martinez-Veracoechea, F. J.; Frenkel, D. Receptor-mediated endocytosis of nanoparticles of various shapes. *Nano Lett.* **2011**, *11*, 5391–5395.

[38] Vácha, R.; Martinez-Veracoechea, F. J.; Frenkel, D. Intracellular release of endocytosed nanoparticles upon a change of ligand–receptor interaction. *ACS Nano* **2012**, *6*, 10598–10605.

[39] Yue, T. T.; Zhang, X. R. Cooperative effect in receptor-mediated endocytosis of multiple nanoparticles. *ACS Nano* **2012**, *6*, 3196–3205.

[40] Li, Y.; Yue, T. T.; Yang, K.; Zhang, X. R. Molecular modeling of the relationship between nanoparticle shape anisotropy and endocytosis kinetics. *Biomaterials* **2012**, *33*, 4965–4973.

[41] Huang, C. J.; Zhang, Y.; Yuan, H. Y.; Gao, H. J.; Zhang, S. L. Role of nanoparticle geometry in endocytosis: Laying down to stand up. *Nano Lett.* **2013**, *13*, 4546–4550.

[42] Yang, K.; Ma, Y.-Q. Computer simulation of the translocation of nanoparticles with different shapes across a lipid bilayer. *Nat. Nanotechnol.* **2010**, *5*, 579–583.

[43] Ding, H.-M.; Tian, W.-D.; Ma, Y.-Q. Designing nanoparticle translocation through membranes by computer simulations. *ACS Nano* **2012**, *6*, 1230–1238.

[44] Ding, H.-M.; Ma, Y.-Q. Controlling cellular uptake of nanoparticles with pH-sensitive polymers. *Sci. Rep.* **2013**, *3*, 2804.

[45] Berendsen, H. J. C.; Postma, J. P. M.; van Gunsteren, W. F.; DiNola, A.; Haak, J. R. Molecular dynamics with coupling to an external bath. *J. Chem. Phys.* **1984**, *81*, 3684–3690.

[46] Humphrey, W.; Dalke, A.; Schulten, K. VMD: Visual molecular dynamics. *J. Mol. Graph.* **1996**, *14*, 33–38.

[47] Hess, B.; Kutzner, C.; van der Spoel, D.; Lindahl, E. GROMACS 4: Algorithms for highly efficient, load-balanced, and scalable molecular simulation. *J. Chem. Theory Comput.* **2008**, *4*, 435–447.

[48] Koynova, R.; Caffrey, M. Phases and phase transitions of the phosphatidylcholines. *Biochim. Biophys. Acta* **1998**, *1376*, 91–145.

[49] Nagle, J. F.; Tristram-Nagle, S. Structure of lipid bilayers. *Biochim. Biophys. Acta* **2000**, *1469*, 159–195.

[50] Kong, X.; Qin, S. S.; Lu, D. N.; Liu, Z. Surface tension effects on the phase transition of a DPPC bilayer with and without protein: A molecular dynamics simulation. *Phys. Chem. Chem. Phys.* **2014**, *16*, 8434–8440.

[51] Marrink, S. J.; Risselada, J.; Mark, A. E. Simulation of gel phase formation and melting in lipid bilayers using a coarse grained model. *Chem. Phys. Lipids* **2005**, *135*, 223–244.

[52] Marrink, S. J.; de Vries, A. H.; Mark, A. E. Coarse grained model for semiquantitative lipid simulations. *J. Phys. Chem. B* **2004**, *108*, 750–760.

[53] Mecke, A.; Majoros, I. J.; Patri, A. K.; Baker Jr, J. R.; Holl, M. M. B.; Orr, B. G. Lipid bilayer disruption by polycationic polymers: The roles of size and chemical functional group. *Langmuir* **2005**, *21*, 10348–10354.

[54] Shen, C. Y.; Lazouskaya, V.; Zhang, H. Y.; Wang, F.; Li, B. G.; Jin, Y.; Huang, Y. F. Theoretical and experimental investigation of detachment of colloids from rough collector surfaces. *Colloid Surf. A* **2012**, *410*, 98–110.

[55] Shen, C. Y.; Wang, F.; Li, B. G.; Jin, Y.; Wang, L.-P.; Huang, Y. F. Application of DLVO energy map to evaluate interactions between spherical colloids and rough surfaces. *Langmuir* **2012**, *28*, 14681–14692.

[56] Shen, C. Y.; Lazouskaya, V.; Zhang, H. Y.; Li, B. G.; Jin, Y.; Huang, Y. F. Influence of surface chemical heterogeneity on attachment and detachment of microparticles. *Colloid Surf. A* **2013**, *433*, 14–29.